CRYSTAL GROWTH & DESIGN

pubs.acs.org/crystal

Article

Temozolomide–Hesperetin Drug–Drug Cocrystal with Optimized Performance in Stability, Dissolution, and Tabletability

Jie Wang, Xia-Lin Dai,* Tong-Bu Lu, and Jia-Mei Chen*

Cite This: *Cryst. Growth Des.* 2021, 21, 838–846

Read Online

ACCESS | Metrics & More | Article Recommendations | Supporting Information

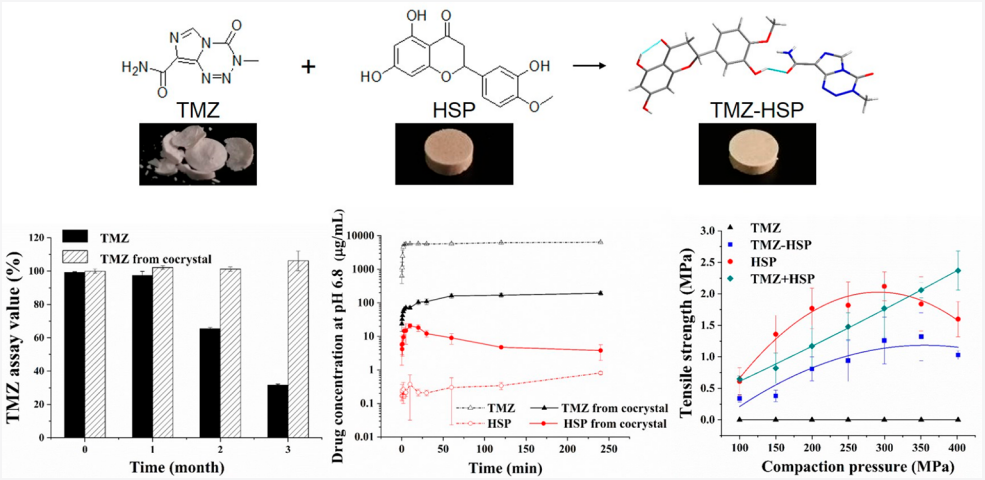

ABSTRACT: A new 1:1 drug–drug cocrystal of temozolomide and hesperetin was successfully prepared by liquid-assisted grinding, slurry conversion crystallization, and evaporation crystallization. The obtained cocrystal was comprehensively characterized by single-crystal and powder X-ray diffraction, differential scanning calorimetry, and thermogravimetric analysis, as well as by Fourier transform infrared and nuclear magnetic resonance spectroscopy. The two drug molecules in the cocrystal are connected via O–H···O hydrogen bonds between the carbonyl oxygen of temozolomide and the phenolic hydroxyl group of hesperetin. The drug–drug cocrystal enhances the hydroscopic stability of hesperetin and the physicochemical stability of temozolomide. In addition, the cocrystal optimizes the dissolution behavior of temozolomide and hesperetin at pH 1.2 and pH 6.8 in comparison to the pristine drugs. Further, a compressibility assessment was also conducted, and the cocrystal exhibits a superior tabletability in comparison with temozolomide. Therefore, the drug–drug cocrystal has the potential to be developed as an efficient oral formulation of a drug combination which will overcome the weaknesses of each parent drug.

INTRODUCTION

Pharmaceutical cocrystals are defined as homogeneous crystalline solids composed of an active pharmaceutical ingredient (API) and pharmaceutically acceptable cocrystal formers (CCFs), wherein the API and CCFs are combined in the same crystal lattice via noncovalent interactions in a stoichiometric ratio.[1] The formation of cocrystals offers an opportunity to ameliorate the physical and chemical properties, including stability, solubility, dissolution rate, bioavailability, tabletability, etc., of a given API without changing the covalent bonding structure.[2−7] Drug–drug cocrystals are an emergent subset of cocrystals, which are composed of two different API molecules. In comparison to the parent drugs, drug–drug cocrystals exhibit many advantages, such as the amelioration of the physicochemical properties of each component and the opportunity for the development of synergistic therapies.[8,9] Moreover, they also provide an attractive avenue to expand the intellectual property and enable the life cycle management of drug products.[10] Therefore, drug–drug cocrystals have captured growing interest in the pharmaceutical industry. However, this field remains underexplored at present due to the complexity in the rational design and development.

Temozolomide (TMZ, Scheme 1) is an oral alkylating agent used to treat malignant gliomas.[11,12] TMZ is a prodrug that spontaneously hydrolyzes into the active compound 5-(3-monomethyl-1-triazeno)imidazole-4-carboxamide (MTIC)

Received: August 17, 2020
Revised: December 18, 2020
Published: January 2, 2021

Scheme 1. Chemical Structures of TMZ and HSP

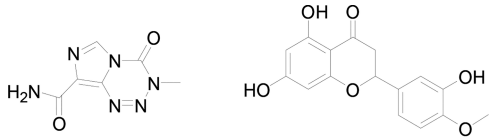

under physiological conditions (Scheme S1 in the Supporting Information). MTIC further decomposes into 5-amino-imidazole-4-carboxamide (AIC) and methyldiazonium cation ($CH_3N_2^+$), the latter of which is an active alkylated substance that exerts antitumor efficiency through DNA methylation.[13] Currently, TMZ is a first-line chemotherapy drug for the treatment of malignant glioma.[14] However, the efficacy of TMZ is limited due to its rapid elimination after oral administration. In addition, TMZ suffers from stability issues, as it degrades into AIC during storage and processing, which also reduces the effectiveness of the drug. Some cocrystals of TMZ with succinic acid, oxalic acid, isonicotinamide, nicotinamide, pyrazinamide, 4-hydroxybenzamide, etc. have been studied and have demonstrated improved stability.[15−17] Recently, our group reported a drug−drug cocrystal involving TMZ and baicalein (BAI), which shows optimized stability, solubility, and pharmacokinetics in comparison to the two parent drugs.[18] This encouraged us to explore more drug−drug cocrystals of TMZ with other flavonoid active ingredients to provide more options for potential clinical applications. Hence, a series of flavonoid compounds with antiglioma activity, including apigenin, daidzein, hesperetin, morin, naringenin, puerarin, etc., were selected to cocrystallize with TMZ. Finally, a drug−drug cocrystal of TMZ with hesperetin (HSP, Scheme 1) was obtained.

HSP is a compound found in citrus fruits which possesses extensive pharmacological effects, such as antioxidant, anticarcinogenic, anti-inflammatory, antibacterial, antiallergic, and antitumor activities.[19−22] In contrast to BAI, which suppresses cell proliferation, promotes apoptosis, and arrests the cell cycle by reducing the expression of HIF-1α, VEGF, and VEGFR2 in U87 gliomas,[23] HSP induces the apoptosis of glioma cells by activating p38 MAPK and thereby possesses a totally different antiglioma mechanism.[24] In addition, HSP does not accumulate in any organs and is safe to be used with negligible toxicity.[25] Therefore, it has the potential to cooperate with TMZ to exert synergistic effects in the treatment of malignant glioma with different potential therapeutic effects and can be applied to different clinic settings in comparison to **TMZ-BAI**. However, HSP has the weakness of poor solubility similar to that of BAI, which consequently leads to low bioavailability in living organisms and further limits its potential as an active antitumor drug.[26,27] Cocrystal formation of HSP with picolinic acid, nicotinamide, and caffeine has already been proved to be an effective method to improve its solubility and oral bioavailability.[28]

In the present work, we focused on a drug−drug cocrystal of TMZ and HSP (**TMZ-HSP**), aiming to optimize the properties of both drugs for the synergistic treatment of glioma. Although TMZ possesses three anhydrous polymorphs and one monohydrate form[29,30] and HSP has one anhydrous form and one monohydrate form,[31,32] no polymorphism phenomenon was observed during the cocrystallization of TMZ and HSP and only one cocrystal form was obtained in the present study. The cocrystal was prepared by multiple methods and characterized comprehensively. The crystal structure was successfully determined by single-crystal X-ray diffraction. Furthermore, the pharmaceutical properties, including physicochemical stability, dissolution characteristics, and tabletability of the cocrystal, were also investigated to evaluate the pharmaceutical applicability.

RESULTS AND DISCUSSION

Crystal Structure Analysis. Single-crystal X-ray diffraction (SCXRD) can elucidate the three-dimensional (3D) structure of cocrystals, including the supramolecular synthons and crystal-packing details.[33] The crystal structure of **TMZ-HSP** was determined by SCXRD at 293 K. The crystallographic data and refinement details are provided in Table 1. The selected

Table 1. Crystallographic Data and Refinement Parameters for TMZ-HSP

chem formula	$C_{22}H_{20}N_6O_8$
formula wt	496.44
temp (K)	293(2)
λ (Å)	0.71073
cryst size (mm^3)	0.10 × 0.05 × 0.03
cryst syst	orthorhombic
space group	$Pca2_1$
a (Å)	37.3480(4)
b (Å)	7.3427(9)
c (Å)	8.1247(11)
α (deg)	90.00
β (deg)	90.00
γ (deg)	90.00
V (Å^3)	2228.1(5)
Z	4
calcd density (g/cm^3)	1.480
θ range for data collection (deg)	2.734−27.499
F(000)	1032.0
index ranges	$-48 \le h \le 48$
	$-9 \le k \le 9$
	$-10 \le l \le 10$
no. of reflns	5123
no. of unique reflns	4495
no. of params	341
$R1_{all}$, $R1_{obs}$ [a]	0.0951, 0.0879
$wR2_{all}$, $wR2_{obs}$ [b]	0.2141, 0.2086
GOF	1.061
CCDC no.	1985464

[a] $R1 = \sum||F_o| - |F_c||/\sum|F_o|$. [b] $wR2 = [\sum[w(F_o^2 - F_c^2)^2]/\sum w(F_o^2)^2]^{1/2}$, $w = 1/[\sigma^2(F_o)^2 + (aP)^2 + bP]$, where $P = [(F_o^2) + 2F_c^2]/3$.

Table 2. Hydrogen-Bonding Distances and Angles for TMZ-HSP

hydrogen bond	H···A (Å)	D···A (Å)	∠D−H···A (deg)	symmetry code
O3−H3···O2	1.93	2.627(7)	143.1	
O4−H4···O2	1.97	2.762(7)	163.9	$-x - 3/2, y + 1, z - 1/2$
O5−H5···O7	1.99	2.852(8)	142.0	
N6−H6A···O7	2.09	2.849(9)	146.6	$-x - 1, -y - 1, z + 1/2$

https://dx.doi.org/10.1021/acs.cgd.0c01153
Cryst. Growth Des. 2021, 21, 838−846

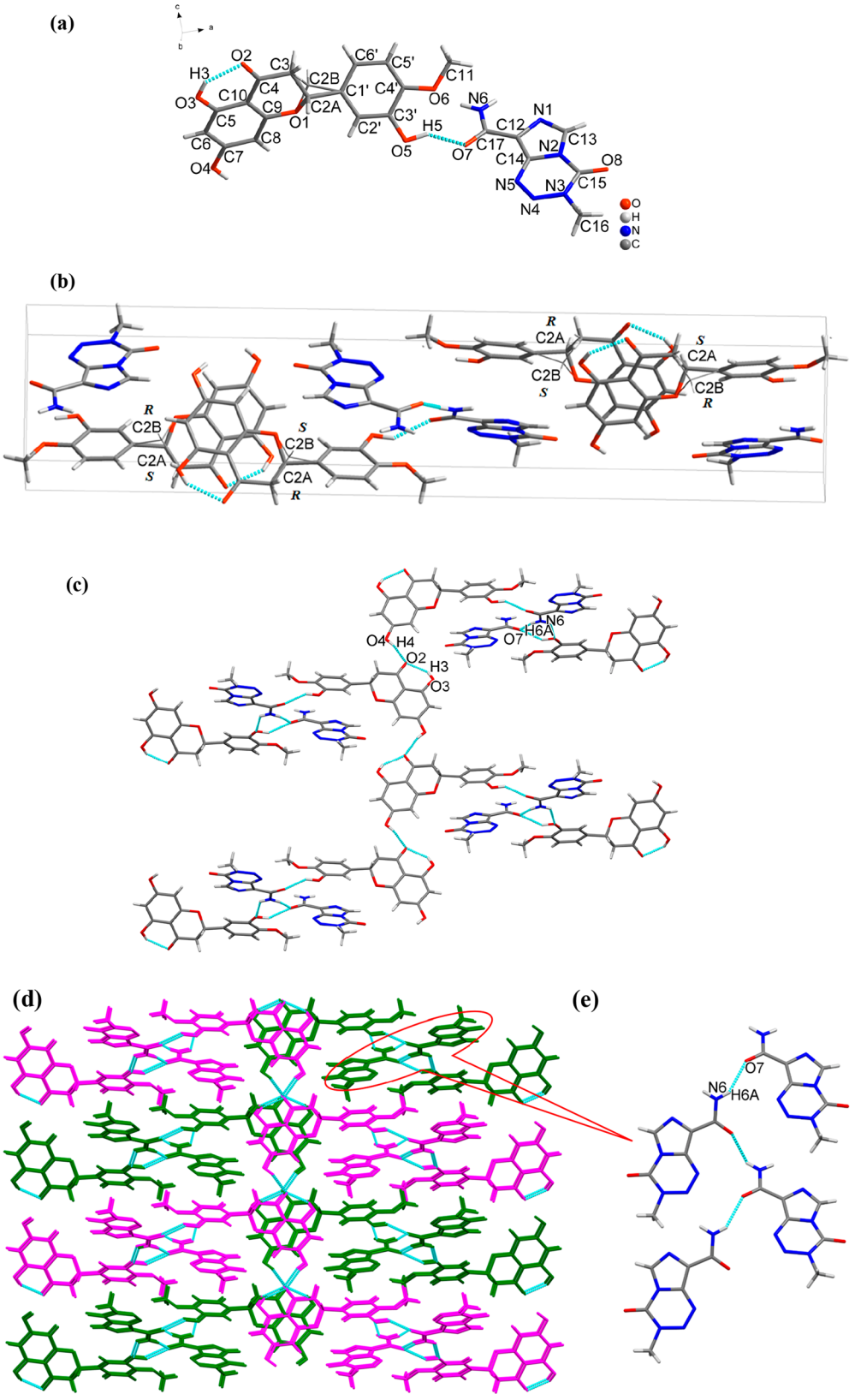

Figure 1. (a) Asymmetric unit, (b) cell packing, (c) 2D and (d) 3D hydrogen-bonded frameworks of **TMZ-HSP**, and (e) 1D hydrogen-bonded chain of TMZ.

hydrogen-bonding angles and distances are given in Table 2. **TMZ-HSP** crystallizes in the orthorhombic space group $Pca2_1$, with one molecule each of TMZ and HSP in the asymmetric unit (Figure 1a). The C2 atom of the HSP molecule is a chiral center, which is disordered over two positions with an occupancy ratio of 0.75:0.25 (for C2A and C2B, respectively). There are four HSP molecules in the crystal cell, among which the C2A and C2B atoms of two HSP molecules correspond to

https://dx.doi.org/10.1021/acs.cgd.0c01153
Cryst. Growth Des. 2021, 21, 838−846

R and *S* enantiomers, respectively. For the other two HSP molecules, the C2A and C2B atoms are representative of *S* and *R* enantiomers, respectively (Figure 1b). Overall, the HSP molecules in **TMZ-HSP** are a racemic mixture. There is an intramolecular O3−H3···O2 hydrogen bond between hydroxyl and carbonyl groups in each HSP molecule. TMZ and HSP molecules are connected through an O5−H5···O7 hydrogen bond to form a dimer (Figure 1a). Two dimers are further connected via a N6−H6A···O7 hydrogen bond between amide groups of adjacent TMZ molecules to generate a tetramer. The tetramers are held together through an O4−H4···O2 hydrogen bond between hydroxyl and carbonyl groups of neighboring HSP molecules to generate a one-dimensional (1D) belt (Figure 1c). The belts are further stacked along the *c* axis to form a 3D hydrogen-bonded framework structure (Figure 1d), within which there also exist 1D hydrogen-bonded chain structures of TMZ molecules (Figure 1e).

Powder X-ray Diffraction (PXRD) and Thermal Analyses. PXRD analysis was utilized to identify the crystalline phase and determine the phase purity of the bulk sample of **TMZ-HSP** (Figure 2).[34,35] The PXRD pattern of

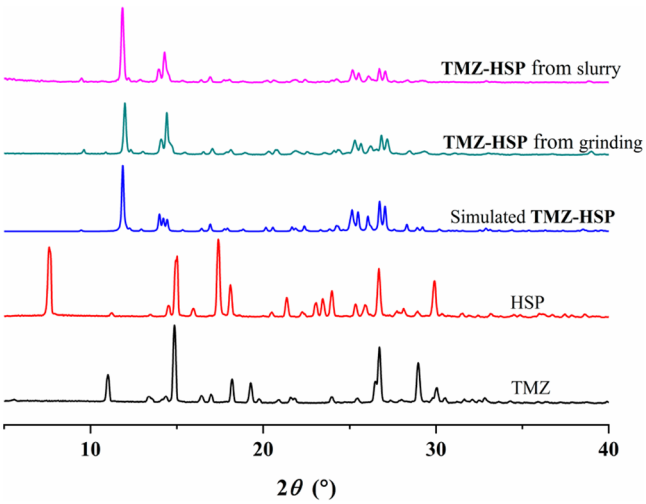

Figure 2. Comparison of experimental and simulated PXRD patterns of **TMZ-HSP**, HSP and TMZ.

synthesized **TMZ-HSP** is distinguished from those of its parent materials, suggesting the formation of a new crystalline phase. Moreover, the experimental PXRD pattern is consistent with the simulated pattern calculated from single-crystal data, confirming the crystalline phase purity of the synthesized cocrystal. The thermodynamic stability of the parent materials and cocrystal was investigated by means of thermogravimetric (TG) and differential scanning calorimetry (DSC) analyses. From TG thermograms it can be seen that TMZ, HSP, and **TMZ-HSP** are free from crystalline water or solvents in the lattice and begin to decompose at approximately 186.8, 276.4, and 199.8 °C, respectively. The DSC curve of HSP shows an endothermic peak of melting at 232.4 °C, while those of TMZ and **TMZ-HSP** show exothermic peaks at 202.2 and 200.9 °C, respectively, corresponding to their decomposition processes (Figure S1 in the Supporting Information). A TG and DSC analysis of the 1:1 physical mixture of TMZ and HSP has also been carried out. The DSC curve of the physical mixture exhibits an endothermic peak at 178.0 °C, which could be ascribed to the formation of a eutectic of TMZ and HSP, and a subsequent exothermic peak at 182.3 °C, which could be attributed to the decomposition of the eutectic (Figure S1 in the Supporting Information).

^{1}H Nuclear Magnetic Resonance (^{1}H NMR). The chemical components in the new cocrystalline phase were further identified and confirmed by ^{1}H NMR. The ^{1}H NMR spectrum of synthesized **TMZ-HSP** was the superposition of the peaks of TMZ and HSP, except for the peaks of active hydrogen (Figure S2 in the Supporting Information), which indicates the presence of these two components in the new phase. The ^{1}H NMR chemical shift assignments are as follows: peaks of TMZ, δ 8.83 (s, 1H), 7.81 (s, 1H), 7.69 (s, 1H), 3.87 (s, 3H); peaks of HSP, δ 6.91 (dd, J = 25.3, 8.4 Hz, 3H), 5.89 (dd, J = 5.6, 2.1 Hz, 2H), 5.42 (dd, J = 12.3, 3.0 Hz, 1H), 3.78 (s, 3H), 3.17 (dd, J = 17.1, 12.4 Hz, 1H), 2.72 (dd, J = 17.1, 3.1 Hz, 1H). The ratio of TMZ and HSP in the cocrystal was calculated to be 1:1 by integrating the characteristic proton signals of each component.

Fourier Transform Infrared Spectroscopy (FTIR) Analysis. FTIR spectra can further identify the intermolecular interactions of functional groups involved by the changes in their vibrational frequencies. The FTIR spectra for TMZ, HSP, **TMZ-HSP**, and the corresponding physical mixture are presented in Figure 3. HSP shows characteristic peaks at

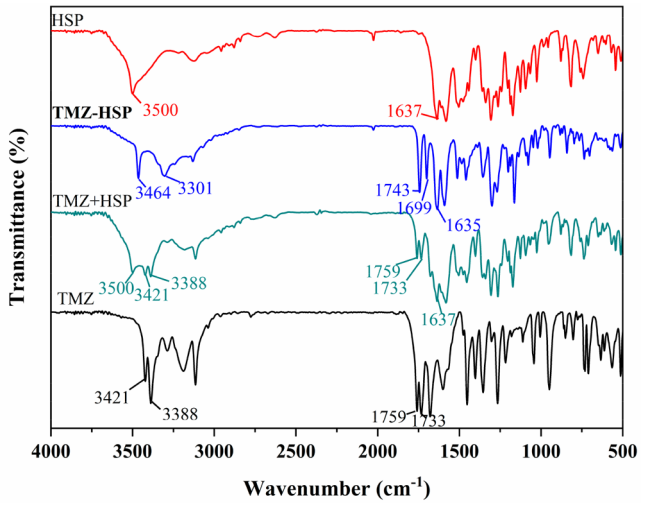

Figure 3. FTIR spectra of TMZ, HSP, **TMZ-HSP**, and a physical mixture (TMZ + HSP).

1637 and 3500 cm^{-1}, which are assigned to the carbonyl C═O and O−H stretching vibrations.[36] The N−H stretching of TMZ exhibits characteristic peaks at 3421 and 3388 cm^{-1}, and the stretching vibrations at 1759 and 1733 cm^{-1} correspond to the C═O stretching vibrations from the primary and tertiary amides of TMZ, respectively.[37] After the formation of **TMZ-HSP**, the C═O stretching vibrations were observed at 1635, 1699, and 1743 cm^{-1} and the O−H and N−H stretchings were shifted to 3464 and 3301 cm^{-1}, respectively. These spectral peak shifts reflect that the amide groups of TMZ and the hydroxyl and carbonyl groups of HSP participate in the change in hydrogen-bonding modes accompanying cocrystal formation.

Dynamic Vapor Sorption (DVS) Study. A DVS study was carried out to compare the hygroscopicity of **TMZ-HSP** with those of the parent TMZ and HSP. The resulting vapor sorption/desorption isotherms are depicted in Figure 4. The

https://dx.doi.org/10.1021/acs.cgd.0c01153
Cryst. Growth Des. 2021, 21, 838−846

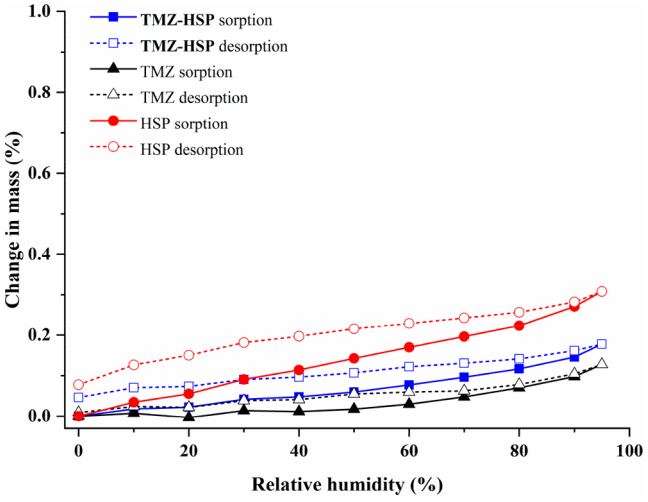

Figure 4. Water sorption/desorption isotherms for TMZ, HSP, and **TMZ-HSP** at 25 °C.

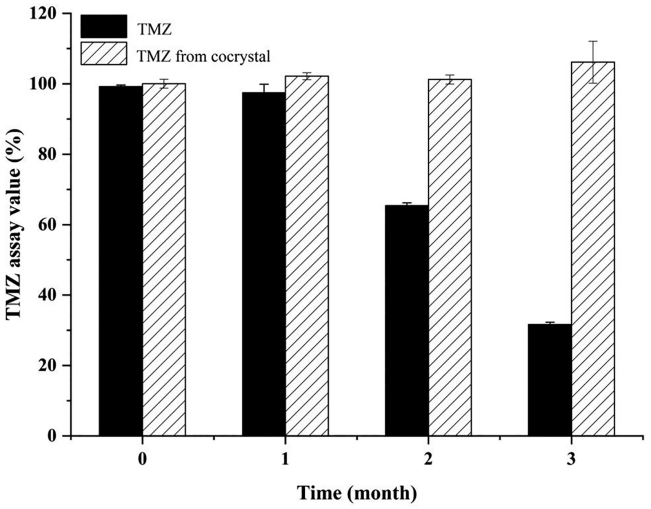

Figure 5. Changes in TMZ assay values during storage under 40 °C/75% RH for TMZ and **TMZ-HSP** (n = 3).

possible phase transitions during the DVS experiments were monitored by PXRD detection. **TMZ-HSP** absorbs more water than pure TMZ but absorbs less water than the parent HSP at all relative humidity (RH) levels. The absorption quantity of water molecules at 95% RH for **TMZ-HSP** is 0.18%, which could be considered as nonhygroscopic.[38] As the humidity drops back to 0% RH, all of the samples lose the absorbed water reversibly and no hysteresis gap was observed. The results reveal that there is no phase transition for the three samples under the experimental conditions. The PXRD patterns of TMZ, HSP, and **TMZ-HSP** after DVS experiments further confirm that all the samples kept their original crystalline phases (Figure S3 in the Supporting Information).

Accelerated Stability Test. Cocrystal formation can modulate the physical and chemical stability of the involved compounds by changing the molecular arrangements and packing patterns. TMZ suffers from chemical stability issues, as it tends to degrade to form AIC during storage processing; thus, chemical stability tests of TMZ and **TMZ-HSP** were performed under accelerated ICH conditions (40 °C/75% RH) with time intervals of 1, 2, and 3 months to better observe and compare the degradation process of TMZ. The results show that the parent TMZ powder changed from white to pink within 1 month and further turned into dark brown after 3 months, confirming that TMZ degraded under 40 °C/75% RH as previously reported (Figure S4 in the Supporting Information).[39,40] PXRD measurements demonstrate that TMZ was partially degraded with undesired peaks appearing at 2θ values of 11.6, 12.9, and 27.3° after 2 months, and some peaks appeared at 11.2, 12.9, 15.2, 27.0, and 27.8° after 3 months (Figure S5 in the Supporting Information). The sample of TMZ after 3 months of storage was then studied by a ^{1}H NMR analysis. The results show that it was a mixture of TMZ and AIC as well as a small amount of other impurities, which are consistent with the results of HPLC analysis (Figures S6 and S7 in the Supporting Information). In addition, the content of TMZ decreased sharply to 65.43 ± 0.76% and 31.64 ± 0.64% after 2 and 3 months, respectively (Figure 5). In comparison, the cocrystal demonstrates neither a color change nor a crystalline phase transformation under the same conditions until the end of the third month (Figures S4 and S5 in the Supporting Information). Moreover, it also shows a remarkably higher content of TMZ at all sampling points (Figure 5). The stability test concludes that **TMZ-HSP** exhibits significantly improved physical and chemical stability in comparison with parent TMZ. This could be attributed to the modulation of crystal structure and intermolecular interactions after cocrystallization. In the crystal structure of pure TMZ, the C═O group of the tertiary amide forms a hydrogen bond with the NH_2 group, which may promote the hydrolysis of TMZ. In contrast, the C═O group of the tertiary amide in **TMZ-HSP** is free from hydrogen-bonding interactions, which will not advance the hydrolysis of TMZ and thereby improve its stability. A similar phenomenon has also been observed in the cocrystal of temozolomide and baicalein.[18]

Dissolution Study. The apparent solubility and dissolution rate of solid-state drugs have an important effect on their *in vivo* release and absorption and further affect their effectiveness and safety.[41−43] The powder dissolutions of TMZ, HSP, and **TMZ-HSP** were investigated at pH 1.2 and pH 6.8 (Figure 6). Pure TMZ exhibits a higher solubility with a maximum apparent solubility (S_{max}) of 7600 μg/mL (at pH 1.2) and 6424 μg/mL (at pH 6.8) (Table 3). The good aqueous solubility of TMZ may lead to its rapid absorption and short retention time *in vivo*. After the formation of **TMZ-HSP**, the S_{max} of TMZ was effectively reduced to 483.9 and 193.5 μg/mL at pH 1.2 and pH 6.8, respectively, which is consistent with the reported solubility decrease of TMZ from **TMZ-BAI** (Figure 6a).[18] Thus, it can be inferred that the formation of **TMZ-HSP** may also help to slow the release and absorption of TMZ and prolong its retention time *in vivo* as does **TMZ-BAI**. In contrast, pure HSP is insoluble in water and its S_{max} is only 1.8 μg/mL (at pH 1.2) and 0.8 μg/mL (at pH 6.8) (Table 3). The limited aqueous solubility of HSP leads to its low oral bioavailability. For **TMZ-HSP**, the S_{max} of HSP was significantly increased by 17.8 (at pH 1.2) and 26.3 (at pH 6.8) times, which is also similar to the enhanced solubility of BAI for the reported **TMZ-BAI**, indicating that the solubility increase of HSP herein has the potential to transform into the improvement of its oral bioavailability (Figure 6b). The modulation of solubility of a multicomponent crystal is relative to the affinity of each component to the media. The cocrystal formation between hydrophilic TMZ and hydrophobic HSP

https://dx.doi.org/10.1021/acs.cgd.0c01153
Cryst. Growth Des. 2021, 21, 838−846

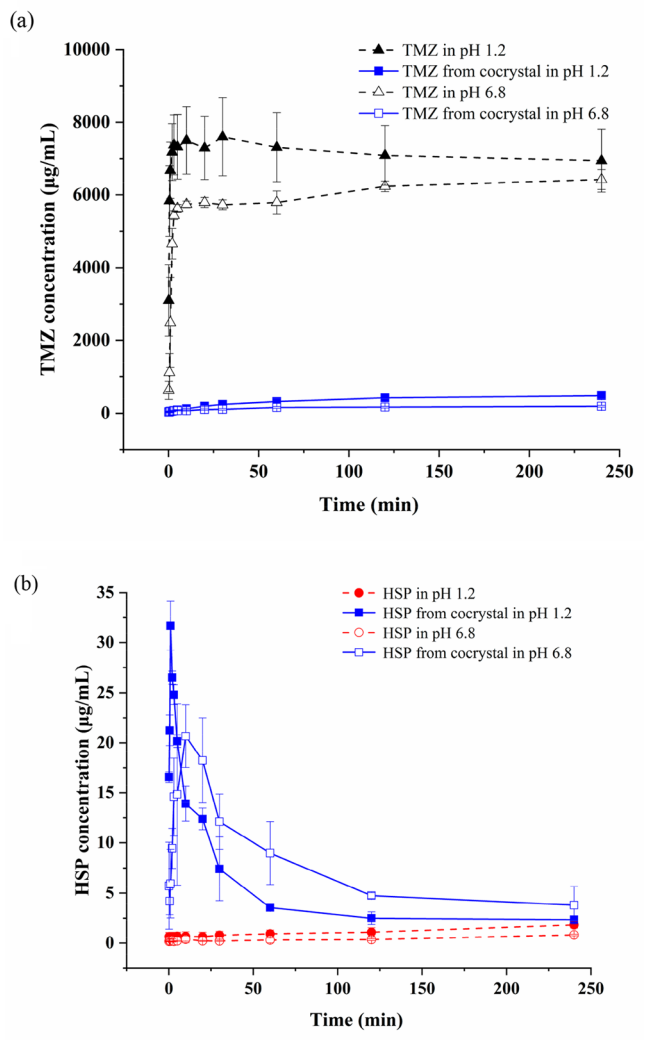

Figure 6. Powder dissolution profiles of (a) TMZ and **TMZ-HSP** and (b) HSP and **TMZ-HSP** at 37 °C.

Table 3. S_{max} Values of TMZ and HSP in HCl Solution (pH 1.2) and PBS Solution (pH 6.8)

	S_{max} (μg/mL)	
sample	pH 1.2	pH 6.8
TMZ	7600 (1071)	6424 (277)
TMZ from cocrystal	483.9 (11.1)	193.5 (23.9)
HSP	1.8 (0.3)	0.8 (0.1)
HSP from cocrystal	32 (3)	21 (3)

may reduce the hydrophilicity of TMZ and improve the hydrophilicity of HSP. This thereby results in the decreased aqueous solubility of TMZ and the increased aqueous solubility of HSP at the same time.

In addition, the pure TMZ and HSP demonstrate great difference in solubility at either pH 1.2 or pH 6.8, which may lead to compatibility issues when they are given in combination with the form of a physical mixture. In comparison, after the formation of **TMZ-HSP**, the solubility difference between TMZ and HSP was substantially reduced (Table 3). This means that the drug−drug cocrystal is a better alternative for the development of combination preparations of TMZ and HSP.

The crystalline phases of the remaining solids and the pH values of the dissolution media were also examined after powder dissolution experiments. At pH 1.2, TMZ was transformed into TMZ monohydrate, while the crystal forms of HSP and **TMZ-HSP** remained unchanged (Figure S8 in the Supporting Information). The pH values of the dissolution media of all samples were changed to 1.3−1.4, which could be attributed to the weak basicity of TMZ and HSP.[44] At pH 6.8, the PXRD pattern of TMZ after dissolution is similar to that of TMZ after the accelerated stability test, suggesting that TMZ was also partially degraded during dissolution (Figure S8 in the Supporting Information). The sample of TMZ after dissolution was further proved to be a mixture of TMZ, AIC, and a small amount of other impurities by ^{1}H NMR analysis (Figure S9 in the Supporting Information). The crystal form of HSP remained unchanged, while a small amount of diffraction peaks of HSP·H_2O appeared for the cocrystal phase (Figure S8 in the Supporting Information). The pH values of the dissolution media for all of the samples remained unchanged.

Compaction Property. Cocrystal formation can modulate the compaction property and therefore the manufacturability of solid-state drugs.[45,46] Tabletability refers to the ability of the bulk powders of a drug to be transformed into a tablet with a specific tensile strength over a certain compaction pressure.[47,48] In this study, the tabletabilities of TMZ, HSP, **TMZ-HSP**, and a 1:1 physical mixture of TMZ and HSP (TMZ + HSP) were determined under a compaction pressure from 100 to 400 MPa. TMZ powders cannot form intact tablets under a compaction pressure up to 400 MPa, and tablet lamination and capping were observed. In comparison to the poor compaction property of TMZ powder, HSP, **TMZ-HSP**, and TMZ + HSP powders exhibit much better tableting behavior. They can be made into intact tablets over the entire compaction pressure range without the need for any excipients. In addition, these tablets remained intact after 24 h of relaxation without evidence of delamination or capping. A typical tablet of each sample compressed at 400 MPa is presented in Figure 7.

The tabletability profiles of the four powdered samples are shown in Figure 8. The tablet tensile strength of **TMZ-HSP** is much higher than that of TMZ but relatively lower than that of pure HSP under the same compaction pressures. The tablet

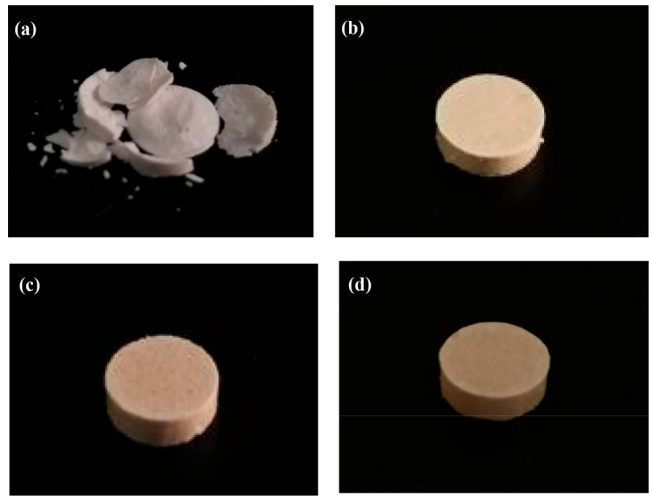

Figure 7. (a) TMZ, (b) **TMZ-HSP**, (c) HSP, and (d) physical mixture (TMZ + HSP) tablets under a compaction pressure of 400 MPa.

https://dx.doi.org/10.1021/acs.cgd.0c01153
Cryst. Growth Des. 2021, 21, 838−846

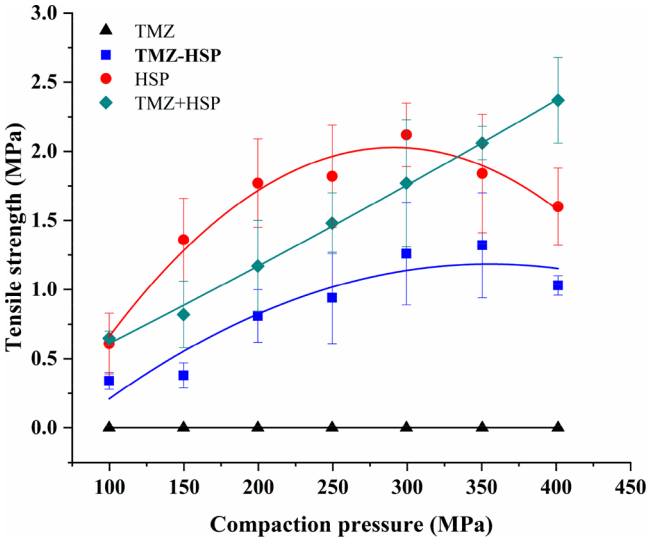

Figure 8. Tabletability profile of TMZ, HSP, **TMZ-HSP**, and a physical mixture (TMZ + HSP).

tensile strengths of HSP and **TMZ-HSP** are increased with an increase of compaction pressure from 100 to 300 and 350 MPa, respectively. However, a further increase in compaction pressure results in a decrease in tensile strength. This phenomenon is known as overcompaction.[49,50] The tablet tensile strength of TMZ + HSP increases with the increase of compaction pressure over the entire pressure range and is even better than that of pure HSP above 350 MPa. Although the tensile strength of **TMZ-HSP** is below 2 MPa, it is still significantly improved in comparison to pure TMZ.

The tabletability of crystalline powders is relative to the molecular arrangements and packing modes of the crystals. The crystal structure of TMZ is packed in a reticular structure without potential slip planes (Figure S10a in the Supporting Information), which makes it difficult to plastically deform and leads to poor tabletability. The crystal structure of HSP is packed by 2D layered structures (Figure S10b in the Supporting Information), which can form slip planes and thereby shows much better tabletability in comparison to TMZ. After the formation of **TMZ-HSP**, the original crystal structures of TMZ and HSP were broken, and the reconstructed crystal structure partially retained 2D layered structures formed by HSP molecules and showed a hydrogen-bonded network formed by TMZ and HSP at the same time (Figure S10c in the Supporting Information). Therefore, the cocrystal demonstrates tabletability intermediate between those of pure TMZ and HSP.

After experiments, the powders of HSP, **TMZ-HSP**, and TMZ + HSP were collected and determined by PXRD. The results reveal that there was no stress-induced polymorphic transition during the compaction process (Figure S11 in the Supporting Information).

CONCLUSION

In summary, a drug−drug cocrystal composed of TMZ and HSP (**TMZ-HSP**) with a 1:1 stoichiometric ratio was constructed in order to overcome the deficiencies of individual APIs and realize drug combination at a molecular level. The cocrystal can be prepared by liquid-assisted grinding, slurry conversion crystallization, and evaporation crystallization and was fully characterized by X-ray diffraction, thermal analyses, and Fourier transform infrared and nuclear magnetic resonance spectroscopy. The two drug molecules in the cocrystal are connected by O−H···O hydrogen bonds between the carbonyl oxygen of TMZ and the phenolic hydroxyl group of HSP. The stability, dissolution, and compaction evaluations highlight that the formation of **TMZ-HSP** not only improves the physicochemical stability and tabletability of TMZ but also optimizes the dissolution behavior and diminishes the solubility difference between TMZ and HSP. Therefore, **TMZ-HSP** has the potential to be developed as an efficient oral formulation of a drug combination containing TMZ and HSP.

ASSOCIATED CONTENT

Supporting Information

The Supporting Information is available free of charge at https://pubs.acs.org/doi/10.1021/acs.cgd.0c01153.

Experimental details, chemical structures of TMZ, MTIC, and AIC, DSC and TG thermoanalytical details, ^{1}H NMR spectroscopy, PXRD analysis with regard to DVS, dissolution and compaction experiments, comparison of color, PXRD patterns and HPLC chromatograms for stability tests, and a comparison of the crystal structures of TMZ, HSP, and **TMZ-HSP** (PDF)

Accession Codes

CCDC 1985464 contains the supplementary crystallographic data for this paper. These data can be obtained free of charge via www.ccdc.cam.ac.uk/data_request/cif, or by emailing data_request@ccdc.cam.ac.uk, or by contacting The Cambridge Crystallographic Data Centre, 12 Union Road, Cambridge CB2 1EZ, UK; fax: +44 1223 336033.

AUTHOR INFORMATION

Corresponding Authors

Xia-Lin Dai − *Tianjin Key Laboratory of Drug Targeting and Bioimaging, School of Chemistry and Chemical Engineering, Tianjin University of Technology, Tianjin 300384, People's Republic of China*; Email: 871098922@qq.com

Jia-Mei Chen − *Tianjin Key Laboratory of Drug Targeting and Bioimaging, School of Chemistry and Chemical Engineering, Tianjin University of Technology, Tianjin 300384, People's Republic of China*; orcid.org/0000-0002-3959-901X; Email: chenjiamei@email.tjut.edu.cn

Authors

Jie Wang − *Institute for New Energy Materials and Low Carbon Technologies, School of Materials Science and Engineering, Tianjin University of Technology, Tianjin 300384, People's Republic of China*

Tong-Bu Lu − *Institute for New Energy Materials and Low Carbon Technologies, School of Materials Science and Engineering, Tianjin University of Technology, Tianjin 300384, People's Republic of China*; orcid.org/0000-0002-6087-4880

Complete contact information is available at: https://pubs.acs.org/10.1021/acs.cgd.0c01153

Notes

The authors declare no competing financial interest.

https://dx.doi.org/10.1021/acs.cgd.0c01153
Cryst. Growth Des. 2021, 21, 838−846

■ ACKNOWLEDGMENTS

This work was financially supported by the National Nature Science Foundation of China (No. 21571194). We thank Ms. Cai-Wen Li of Tianjin University of Technology for assistance in the hardness test of compressed tablets.

■ REFERENCES

(1) Aitipamula, S.; Banerjee, R.; Bansal, A. K.; Biradha, K.; Cheney, M. L.; Choudhury, A. R.; Desiraju, G. R.; Dikundwar, A. G.; Dubey, R.; Duggirala, N.; Ghogale, P. P.; Ghosh, S.; Goswami, P. K.; Goud, N. R.; Jetti, R. R. K. R.; Karpinski, P.; Kaushik, P.; Kumar, D.; Kumar, V.; Moulton, B.; Mukherjee, A.; Mukherjee, G.; Myerson, A. S.; Puri, V.; Ramanan, A.; Rajamannar, T.; Reddy, M.; Rodriguez-Hornedo, N.; Rogers, R. D.; Row, T. N. G.; Sanphui, P.; Shan, N.; Shete, G.; Singh, A.; Sun, C. C.; Swift, J. A.; Thaimattam, R.; Thakur, T. S.; Thaper, R. K.; Thomas, S. P.; Tothadi, S.; Vangala, V. R.; Variankaval, N.; Vishweshwar, P.; Weyna, D. R.; Zaworotko, M. J. Polymorphs, salts, and cocrystals: What's in a name? *Cryst. Growth Des.* **2012**, *12*, 2147−2152.

(2) Thakuria, R.; Delori, A.; Jones, W.; Lipert, M. P.; Roy, L.; Rodriguez-Hornedo, N. Pharmaceutical cocrystals and poorly soluble drugs. *Int. J. Pharm.* **2013**, *453*, 101−125.

(3) Steed, J. W. The role of co-crystals in pharmaceutical design. *Trends Pharmacol. Sci.* **2013**, *34*, 185−193.

(4) Tao, Q.; Chen, J. M.; Ma, L.; Lu, T. B. Phenazopyridine cocrystal and salts that exhibit enhanced solubility and stability. *Cryst. Growth Des.* **2012**, *12*, 3144−3152.

(5) Deng, J. H.; Lu, T. B.; Sun, C. C.; Chen, J. M. Dapagliflozin-citric acid cocrystal showing better solid state properties than dapagliflozin. *Eur. J. Pharm. Sci.* **2017**, *104*, 255−261.

(6) Hiendrawan, S.; Veriansyah, B.; Widjojokusumo, E.; Soewandhi, S. N.; Wikarsa, S.; Tjandrawinata, R. R. Physicochemical and mechanical properties of paracetamol cocrystal with 5-nitroisophthalic acid. *Int. J. Pharm.* **2016**, *497*, 106−113.

(7) Lin, R. Z.; Sun, P. J.; Tao, Q.; Yao, J.; Chen, J. M.; Lu, T. B. Mechanism study on stability enhancement of adefovir dipivoxil by cocrystallization: Degradation kinetics and structure-stability correlation. *Eur. J. Pharm. Sci.* **2016**, *85*, 141−148.

(8) Thipparaboina, R.; Kumar, D.; Chavan, R. B.; Shastri, N. R. Multidrug co-crystals: Towards the development of effective therapeutic hybrids. *Drug Discovery Today* **2016**, *21*, 481−490.

(9) Thakuria, R.; Sarma, B. Drug-drug and drug-nutraceutical cocrystal/salt as alternative medicine for combination therapy: A crystal engineering approach. *Crystals* **2018**, *8*, 101.

(10) Duggirala, N. K.; Perry, M. L.; Almarsson, O.; Zaworotko, M. J. Pharmaceutical cocrystals: Along the path to improved medicines. *Chem. Commun.* **2016**, *52*, 640−655.

(11) Xu, W. L.; Li, T.; Gao, L. S.; Zheng, J. W.; Shao, A. W.; Zhang, J. M. Efficacy and safety of long-term therapy for high-grade glioma with Temozolomide: A meta-analysis. *Oncotarget* **2017**, *8*, 51758−51765.

(12) Newlands, E. S.; Stevens, M. F. G.; Wedge, S. R.; Wheelhouse, R. T.; Brock, C. Temozolomide: A review of its discovery, chemical properties, pre-clinical development and clinical trials. *Cancer Treat. Rev.* **1997**, *23*, 35−61.

(13) Denny, B. J.; Wheelhouse, R. T.; Stevens, M. F. G.; Tsang, L. L. H.; Slack, J. A. NMR and molecular modeling investigation of the mechanism of activation of the antitumor drug Temozolomide and its interaction with DNA. *Biochemistry* **1994**, *33*, 9045−9051.

(14) Karachi, A.; Dastmalchi, F.; Mitchell, D. A.; Rahman, M. Temozolomide for immunomodulation in the treatment of glioblastoma. *Nruro. Oncol.* **2018**, *20*, 1566−1572.

(15) Babu, N. J.; Sanphui, P.; Nangia, A. Crystal engineering of stable Temozolomide cocrystals. *Chem. - Asian J.* **2012**, *7*, 2274−2285.

(16) Sanphui, P.; Babu, N. J.; Nangia, A. Temozolomide cocrystals with carboxamide coformers. *Cryst. Growth Des.* **2013**, *13*, 2208−2219.

(17) Kusuma; Kanakaraju, K.; Lavanya, V.; Nangia, A. Temozolomide cocrystals exhibit drug sensitivity in glioblastoma cells. *Proc. Natl. Acad. Sci., India, Sect. A* **2014**, *84*, 321−330.

(18) Li, J. M.; Dai, X. L.; Li, G. J.; Lu, T. B.; Chen, J. M. Constructing anti-glioma drug combination with optimized properties through cocrystallization. *Cryst. Growth Des.* **2018**, *18*, 4270−4274.

(19) Sheokand, S.; Navik, U.; Bansal, A. K. Nanocrystalline solid dispersions (NSD) of hesperetin (HRN) for prevention of 7, 12-dimethylbenz[a]anthracene (DMBA)-induced breast cancer in Sprague−Dawley (SD) rats. *Eur. J. Pharm. Sci.* **2019**, *128*, 240−249.

(20) Xiong, J.; Zheng, T. J.; Shi, Y.; Wei, F.; Ma, S. C.; He, L.; Wang, S. C.; Liu, X. S. Analysis of the fingerprint profile of bioactive constituents of traditional Chinese medicinal materials derived from animal bile using the HPLC-ELSD and chemometric methods: An application of a reference scaleplate. *J. Pharm. Biomed. Anal.* **2019**, *174*, 50−56.

(21) Wang, J. C.; Zhu, H. L.; Yang, Z. J.; Liu, Z. P. Antioxidative effects of hesperetin against lead acetate-induced oxidative stress in rats. *Indian. J. Pharmacol.* **2013**, *45*, 395−398.

(22) Gonzalez-Gallego, J.; Garcia-Mediavilla, M. V.; Sanchez-Campos, S.; Tunon, M. J. Fruit polyphenols, immunity and inflammation. *Br. J. Nutr.* **2010**, *104*, S15−S27.

(23) Wang, F. R.; Jiang, Y. S. Effect of treatment with baicalein on the intracerebral tumor growth and survival of orthotopic glioma models. *J. Neuro-Oncol.* **2015**, *124*, 5−11.

(24) Li, Q.; Miao, Z. W.; Wang, R.; Yang, J.; Zhang, D. B. Hesperetin induces apoptosis in human glioblastoma cells via p38 MAPK activation. *Nutr. Cancer* **2020**, *72*, 538−545.

(25) Yang, Y. Y.; Bai, L.; Li, X. R.; Xiong, J.; Xu, P. X.; Guo, C. Y.; Xue, M. Transport of active flavonoids, based on cytotoxicity and lipophilicity: An evaluation using the blood-brain barrier cell and Caco-2 cell models. *Toxicol. In Vitro* **2014**, *28*, 388−396.

(26) Guo, J. L.; Tang, W. M.; Lu, S. M.; Fang, Z. X.; Tu, K.; Zheng, M. Y. Solubility improvement of hesperetin by using different octenyl succinic anhydride modified starches. *LWT-Food Sci. Technol.* **2018**, *95*, 255−261.

(27) Lucas-Abellan, C.; Perez-Abril, M.; Castillo, J.; Serrano, A.; Mercader, M.T.; Fortea, M.I.; Gabaldon, J.A.; Nunez-Delicado, E. Effect of temperature, pH, β- and HP-β-cds on the solubility and stability of flavanones: Naringenin and hesperetin. *LWT-Food Sci. Technol.* **2019**, *108*, 233−239.

(28) Chadha, K.; Karan, M.; Bhalla, Y.; Chadha, R.; Khullar, S.; Mandal, S.; Vasisht, K. Cocrystals of hesperetin: Structural, pharmacokinetic, and pharmacodynamic evaluation. *Cryst. Growth Des.* **2017**, *17*, 2386−2405.

(29) Babu, N. J.; Reddy, L. S.; Aitipamula, S.; Nangia, A. Polymorphs and polymorphic cocrystals of Temozolomide. *Chem. - Asian J.* **2008**, *3*, 1122−1133.

(30) Lowe, P. R.; Sansom, C. E.; Schwalbe, C. H.; Stevens, M. F.; Clark, A. S. Antitumor imidazotetrazines. 25. Crystal structure of 8-carbamoyl-3-methylimidazo[5,1-d]-1,2,3,5- tetrazin-4(3H)-one (Temozolomide) and structural comparisons with the related drugs mitozolomide and DTIC. *J. Med. Chem.* **1992**, *35*, 3377−3382.

(31) Shin, W.; Kim, S.; Chun, K. S. Structure of (*R*,*S*)-hesperetin monohydrate. *Acta Crystallogr., Sect. C: Cryst. Struct. Commun.* **1987**, *43*, 1946−1949.

(32) Fujii, S.; Yamagata, Y.; Jin, G. Z.; Tomita, K. Novel molecular conformation of (*R*, *S*)−hesperetin in anhydrous crystal. *Chem. Pharm. Bull.* **1994**, *42*, 1143−1145.

(33) Bredikhin, A. A.; Gubaidullin, A. T.; Bredikhina, Z. A.; Krivolapov, D. B.; Pashagin, A. V.; Litvinov, I. A. Absolute configuration and crystal packing for three chiral drugs prone to spontaneous resolution: Guaifenesin, methocarbamol and mephenesin. *J. Mol. Struct.* **2009**, *920*, 377−382.

(34) Hiendrawan, S.; Hartanti, A. W.; Veriansyah, B.; Widjojokusumo, E.; Tjandrawinata, R. R. Solubility enhancement of ketoconazole via salt and cocrystal formation. *Int. J. Pharm. Pharm. Sci.* **2015**, *7*, 160−164.

https://dx.doi.org/10.1021/acs.cgd.0c01153
Cryst. Growth Des. 2021, 21, 838−846

(35) Sanphui, P.; Goud, N. R.; Khandavilli, U. B. R.; Nangia, A. Fast dissolving curcumin cocrystals. *Cryst. Growth Des.* **2011**, *11*, 4135−4145.
(36) Fathi, M.; Varshosaz, J. Novel hesperetin loaded nanocarriers for food fortification: Production and characterization. *J. Funct. Foods* **2013**, *5*, 1382−1391.
(37) Laszcz, M.; Kubiszewski, M.; Jedynak, L.; Kaczmarska, M.; Kaczmarek, L.; Luniewski, W.; Gabarski, K.; Witkowska, A.; Kuziak, K.; Malinska, M. Identification and physicochemical characteristics of Temozolomide process−related impurities. *Molecules* **2013**, *18*, 15344−15356.
(38) Basavoju, S.; Bostrom, D.; Velaga, S. P. Indomethacin-saccharin cocrystal: Design, synthesis and preliminary pharmaceutical characterization. *Pharm. Res.* **2008**, *25*, 530−541.
(39) Attari, Z.; Rao, C. M.; Kumar, L.; Koteshwara, K. B. Temozolomide and its stability-a critical factor. *Adv. Sci. Lett.* **2017**, *23*, 1841−1845.
(40) Braverman, O.; Feishtein, R.; Weisman, A.; Kaspi, J. Temozolomide storage system. US0222792A1, 2006.
(41) Song, J. X.; Yan, Y.; Yao, J.; Chen, J. M.; Lu, T. B. Improving the solubility of lenalidomide via cocrystals. *Cryst. Growth Des.* **2014**, *14*, 3069−3077.
(42) Chen, J. M.; Wang, Z. Z.; Wu, C. B.; Li, S.; Lu, T. B. Crystal engineering approach to improve the solubility of mebendazole. *CrystEngComm* **2012**, *14*, 6221−6229.
(43) Dai, X. L.; Yao, J.; Wu, C.; Deng, J. H.; Mo, Y. H.; Lu, T. B.; Chen, J. M. Solubility and permeability improvement of allopurinol by cocrystallization. *Cryst. Growth Des.* **2020**, *20*, 5160−5168.
(44) Tsujimoto, M.; Horie, M.; Honda, H.; Takara, K.; Nishiguchi, K. The structure-activity correlation on the inhibitory effects of flavonoids on cytochrome P450 3A activity. *Biol. Pharm. Bull.* **2009**, *32*, 671−676.
(45) Chattoraj, S.; Shi, L.; Sun, C. C. Understanding the relationship between crystal structure, plasticity and compaction behavior of theophylline, methyl gallate, and their 1:1 co−crystal. *CrystEngComm* **2010**, *12*, 2466−2472.
(46) Krishna, G. R.; Shi, L. M.; Bag, P. P.; Sun, C. C.; Reddy, C. M. Correlation among crystal structure, mechanical behavior, and tabletability in the co-crystals of vanillin isomers. *Cryst. Growth Des.* **2015**, *15*, 1827−1832.
(47) Joiris, E.; Martino, P. D.; Berneron, C.; Guyot-Hermann, A. M.; Guyot, J. C. Compression behavior of orthorhombic paracetamol. *Pharm. Res.* **1998**, *15*, 1122−1130.
(48) Tye, C. K.; Sun, C. C.; Amidon, G. E. Evaluation of the effects of tableting speed on the relationships between compaction pressure, tablet tensile strength, and tablet solid fraction. *J. Pharm. Sci.* **2005**, *94*, 465−472.
(49) Sun, C. C. Materials science tetrahedron-a useful tool for pharmaceutical research and development. *J. Pharm. Sci.* **2009**, *98*, 1671−1687.
(50) Sun, C. C. Decoding powder tabletability: Roles of particle adhesion and plasticity. *J. Adhes. Sci. Technol.* **2011**, *25*, 483−499.

https://dx.doi.org/10.1021/acs.cgd.0c01153
Cryst. Growth Des. 2021, 21, 838−846